Integrated Photonic Device for Wavelength-Stable Laser Oscillation and Simultaneous Input Coupling

Keisuke Ozawa , Aika Taniguchi, Ryohei Ueda, Shunsuke Teranishi, Akari Watanabe, Junichi Inoue ,
Kenji Kintaka , *Member, IEEE*, and Shogo Ura, *Member, IEEE*

Abstract—A guided-mode-resonance device for both narrow-band retroreflection and waveguide input coupling was designed and fabricated for operation wavelength of 1550 nm. It consists of a focusing grating coupler (FGC) integrated in a waveguide cavity resonator constructed by a pair of distributed Bragg reflectors (DBRs) on a reflection substrate. The size of the FGC was $31 \times 20 \ \mu m^2$. The device was used as a laser mirror of an external cavity laser. The oscillation wavelength was fixed to the retroreflection wavelength, and the laser power was coupled to a waveguide. The coupled power depends on the length of one DBR. The optimal length for the maximum coupling was also discussed theoretically and experimentally.

Index Terms—External cavity lasers, grating couplers, guided mode resonance, integrated photonics, waveguides.

I. INTRODUCTION

A GUIDED-MODE resonance filter (GMRF) consists of a surface grating on a thin-film waveguide on a transparent substrate and shows a narrowband reflection spectrum for an vertically-incident free-space wave [1], [2], [3], [4], [5], [6], [7]. The grating excites and out-couples a guided wave in a resonance wavelength band. A GMRF has advantages in fabrication convenience and design flexibility in comparison to a dielectric multilayer mirror. A GMRF requires only a few layers whereas a dielectric multilayer mirror requires hundreds of layers for narrowband reflection. Various spectra, including narrowband reflection, narrowband transmission, and wideband reflection, can be obtained by appropriate design of the waveguide structure and grating coupling strength. Narrowband reflection and transmission are useful for laser mirrors [8], [9], [10], [11], [12], [13], [14] and chromatic filters [15], [16], respectively.

Keisuke Ozawa, Aika Taniguchi, Ryohei Ueda, Shunsuke Teranishi, and Akari Watanabe are with the Graduate School of Science and Technology, Kyoto Institute of Technology, Kyoto 606-8585, Japan (e-mail: keichan.228@outlook.jp; m2621028@edu.kit.ac.jp; ueda.kobitennis@gmail.com; m2621030@edu.kit.ac.jp; d1822004@edu.kit.ac.jp).
Junichi Inoue and Shogo Ura are with the Faculty of Electrical Engineering and Electronics, Kyoto Institute of Technology, Kyoto 606-8585, Japan (e-mail: inoue@kit.ac.jp; ura@kit.ac.jp).
Kenji Kintaka is with the Nanomaterials Research Institute, National Institute of Advanced Industrial Science and Technology, Ikeda 563-8577, Japan (e-mail: kintaka.kenji@aist.go.jp).

Wideband reflection is attractive for achromatic mirrors [17], [18]. Moderate bandwidth can be used for color filters [19], [20], [21], [22], [23]. Moreover, intentional introduction of absorptive loss into the guided mode can provide high-extinction absorbers [24], [25]. Since the resonance wavelength is sensitive to an effective refractive index of the guided mode, the GMRF can act as high-precision index sensors applicable to bio-chemical sensing [26], [27]. Another essential feature is polarization selectivity. The GMRF brings not only reflection but also phase shift to only certain polarization component. This feature is exploited for polarizers [28], [29] and depolarizers [30], [31]. Thus, GMRFs have been used as bulk-optic components in most of applications so far. On the other hand, the configuration of guided mode utilization inspires us an application to integrated photonics.

We are investigating utilization of GMR in photonic integrated circuit. However, a normal GMRF needs a sub-millimeter-size interaction aperture for nanometer-order reflection bandwidth. For miniaturizing the aperture, a new type of GMRF, namely, cavity-resonator-integrated guided-mode resonance filter (CRIGF) was proposed [32], [33], [34]. It has a small grating coupler within a waveguide cavity resonator constructed by two distributed Bragg reflectors (DBRs). In addition to the small aperture, the excited guided wave can be extracted from the CRIGF through one of the DBRs [35]. Because of the multi-functionality of input coupling and narrowband reflection, it is expected that a CRIGF serves as an external laser mirror which stabilizes oscillation wavelength to the reflection wavelength and couples the laser light to the waveguide. A combination of semiconductor optical amplifiers (SOAs) integrated on a gain chip and cascaded CRIGFs of different resonance wavelengths integrated on a bus waveguide would provide an ultra-compact multi-wavelength light source without separate multiplexers, such as an arrayed waveguide grating or a multi-mode interference coupler [36]. An SOA and a CRIGF construct a laser cavity. A light launched from an anti-reflection coated facet of the SOA is reflected back by the CRIGF. However, here is an issue to be solved. The diameter of an incident beam to the CRIGF must coincide with the aperture size to obtain high reflectance. The aperture size will be several microns at least even though it is much smaller than GMRF. Meanwhile, a field diameter of the guided mode of an SOA is a few microns. We cannot expect high-efficiency direct butt coupling of the SOA to the CRIGF and need some beam-size conversion.
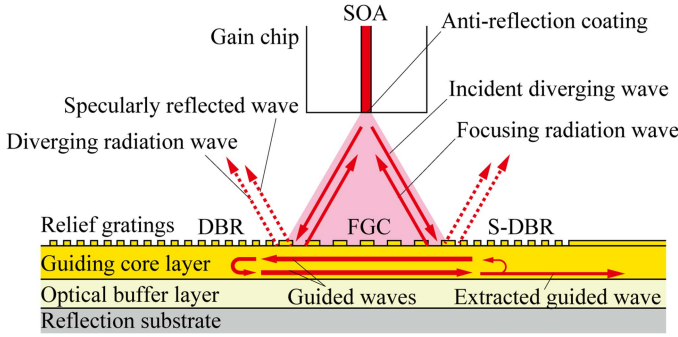
Fig. 1.   Schematic diagram of an external cavity laser using an F-CRIGF.

Fig. 2.   Design example of F-CRIGF.

We proposed a focusing CRIGF (F-CRIGF) for reflecting and focusing a diverging wave back to the diverging point. A focusing grating coupler (FGC) and a reflection substrate are used in the F-CRIGF [37]. An F-CRIGF can retroreflect the emitted light from the SOA. As a result, we can avoid the unpreferable integration of additional lens for the beam-size conversion. Stabilization of oscillation wavelength by an F-CRIGF was demonstrated in previous work [38]. This time, we designed and fabricated F-CRIGFs for input coupling as well as wavelength stabilization. We constructed external-cavity diode lasers (ECDLs) using the F-CRIGFs, and demonstrated wavelength-stable laser oscillation and simultaneous input coupling for the first time. The extraction ratio through one DBR to the waveguide depends on length of the DBR. Shorter DBR gives lower retroreflection to the SOA but higher-efficiency input coupling to the waveguide. We discuss the optimal DBR length with experimental results.

II. Basic Configuration and Operation Principle

Fig. 1 shows a schematic diagram of an ECDL using an F-CRIGF and wave propagation. An F-CRIGF consists of an FGC integrated in a waveguide resonator and an underneath reflection substrate. The waveguide is constructed with an optical buffer layer, a guiding core layer, and relief gratings forming FGC and DBRs [39], [40]. A diverging wave is launched from an anti-reflection coated facet of an SOA. A part of the diverging wave is coupled to counter-propagating guided waves by the FGC in a resonance wavelength band. The rest is specularly reflected by the reflection substrate. The guided waves propagate back and forth in the waveguide resonator. The FGC out-couples the guided waves to diverging and focusing radiation waves depending on the direction of the guided wave propagation. The diverging radiation wave interferes with the specularly reflected wave. They vanish at a wavelength λ_{rc} where complete destructive interference occurs when both DBRs have 100% reflectance. As a result, only the focusing radiation wave remains. The interference destruction degrades in other wavelengths. It means that the maximum retroreflection is obtained at λ_{rc}. Thus, the laser oscillation wavelength is fixed to λ_{rc}. We can extract the resonant guided wave from the F-CRIGF by reducing reflectance of one of DBRs. It is worth noting that the retroreflection for laser oscillation and the excitation of guided mode occur simultaneously. This is a great advantage in integration of an input
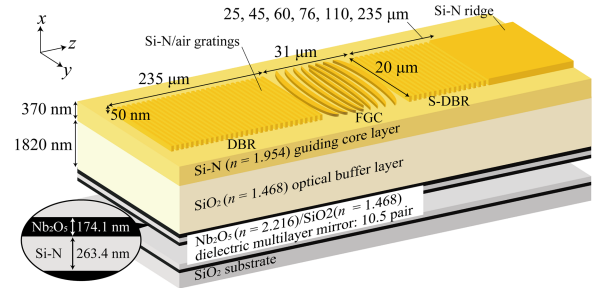
coupler in comparison to a case of usual grating coupler where adjustments in wavelength and incidence-angle are required for high efficiency coupling. You can reduce DBR reflectance by shortening its coupling length. A shortened DBR (S-DBR) is integrated on the side of input coupling port. Shorter S-DBR extracts more guided-wave power, but degrades the guided mode resonance leading to reduction of the retroreflection to the SOA. Therefore, the S-DBR length should be designed to maximize the device efficiency of the guided-mode launching ECDL.

III. Design Example

A. F-CRIGF Structure

Fig. 2 shows a schematic view of the designed F-CRIGF for λ_{rc} of 1550 nm. We assumed y-polarized incident light and designed F-CRIGFs operating with transverse-electric guided mode. A 370-nm-thick Si-N guiding core layer (refractive index of 1.954) and a 1820-nm-thick SiO$_2$ optical buffer layer (refractive index of 1.468) are stacked on a reflection substrate. The reflection substrate is made of a dielectric multilayer mirror of 10.5 pairs of 174.1-nm-thick Nb$_2$O$_5$ (refractive index of 2.216) and 263.4-nm-thick SiO$_2$ deposited on a SiO$_2$ substrate to give 100% reflectance. Si-N/air gratings of 50-nm height are formed on the core layer. The fill factor of the gratings was set to 0.5. The effective refractive index N of the guided mode was estimated to be 1.678 with an assumption of a simplified structure replacing the gratings by a uniform layer with a dielectric-constant-averaged refractive index. Coupling length L_{GC}, width W_{GC}, and focal length f of the FGC were set to 31, 20, and 67 μm, respectively, corresponding to divergence angles from the SOA facet of 17° in z-direction and 27° in y-direction. These angles are the same as the ones of the SOA used in the experiment described in Section IV. Grating line patterns can be expressed with use of difference in spatial phase between the incident and diffracted waves. The phase of $+z$ propagation guided wave ϕ_g can be written as

$$\phi_g = -\frac{2\pi}{\lambda_{rc}} N z. \tag{1}$$

The phase of $-z$ propagation guided wave is $-\phi_g$. The m-th grating line pattern of the DBR reflecting $+z$ propagation guided wave to $-z$ propagation guided wave is expressed by

$$-\phi_g - \phi_g = \frac{4\pi}{\lambda_{rc}} N z = 2\pi m + const. \tag{2}$$

The phase of the incident free space wave diverging from a point $(f, 0, 0)$ to the FGC is expressed by

$$\phi_{in}\ (x,\ y,z) = -\frac{2\pi}{\lambda_{rc}}\sqrt{(x-f)^2 + y^2 + z^2}. \qquad (3)$$

A half part of FGC located in negative z area $(-L_{GC}/2 < z < 0)$ was designed to launch a guided wave propagating $+z$ direction while the other part $(0 < z < L_{GC}/2)$ was designed to launch $-z$ propagating guided wave. The m-th line pattern of the FGC for negative and positive z area on the waveguide plane can be written as

$$\phi_g - \phi_{in}\ (0,\ y,z) = \frac{2\pi}{\lambda_{rc}}\left\{\sqrt{f^2 + y^2 + z^2} - Nz\right\}$$

$$= 2\pi m + f, \qquad (4)$$

$$-\phi_g - \phi_{in}\ (0,\ y,z) = \frac{2\pi}{\lambda_{rc}}\left\{\sqrt{f^2 + y^2 + z^2} + Nz\right\}$$

$$= 2\pi m + f, \qquad (5)$$

respectively. The FGC has curved and chirped pattern [37]. The grating period was calculated to be from 920 to 810 nm in the current case. The grating period of the DBR was determined to be 462.5 nm $(=\lambda_{rc}/2N)$. The distance between the two DBRs must be integer multiple of λ_{rc}/N for occurring retroreflection at λ_{rc} and was set to 32.4 μm $(=35\lambda_{rc}/N)$. The calculated values of reflectances of S-DBRs with coupling lengths of 235, 110, 76, 60, 45, and 25 μm were 0, -0.002, -0.03, -0.11, -0.38, and -2.1 dB, respectively. The 50-nm-thick and 20-μm-wide Si-N ridge are formed on the core layer at an output waveguide to support the extracted guided wave.

B. Theoretically Predicted Characteristics

Reflectance spectra of designed F-CRIGFs were calculated using a model developed by ourselves [41]. Focusing reflectance R_f and specular reflectance R_s of F-CRIGF are given by

$$R_f = \left| \text{sinc}\left(\frac{\Delta L_{GC}}{2}\right)\frac{\pi c}{N}\frac{L_{GC}}{L_{Cav}}\frac{|\kappa_{gd}|^2 r_a + \kappa_{ga}\kappa_{gs}^* t_a E_{\nu a}^0/E_{\nu s}^0}{j(\omega - \omega_{rc}) + 1/\tau}\right|^2, \qquad (6)$$

$$R_s = \left| r_a - \text{sinc}\left(\frac{\Delta L_{GC}}{2}\right)\frac{\pi c}{N}\frac{L_{GC}}{L_{Cav}}\right.$$

$$\left. \times \frac{|\kappa_{ga}|^2 r_a + \kappa_{ga}\kappa_{gs}^* t_a E_{\nu a}^0/E_{\nu s}^0}{j(\omega - \omega_{rc}) + 1/\tau}\right|^2, \qquad (7)$$

$$\frac{1}{\tau} = \frac{c}{N L_{Cav}} \times \left\{ \text{sinc}\left(\frac{\Delta L_{GC}}{2}\right)\alpha L_{GC}\right.$$

$$\left. - \frac{\ln\sqrt{R_{DBR}R_{S-DBR}}}{2}\right\}, \qquad (8)$$

$$\alpha = \pi\left(|\kappa_{ga}|^2 + |\kappa_{gs}|^2\right), \qquad (9)$$

where $c, L_{Cav}, \omega, \omega_{rc}, R_{DBR}$, and R_{S-DBR} are the speed of light in a vacuum, length of the waveguide cavity, angular frequencies of incident-wave wavelength and of λ_{rc} and reflectances of the
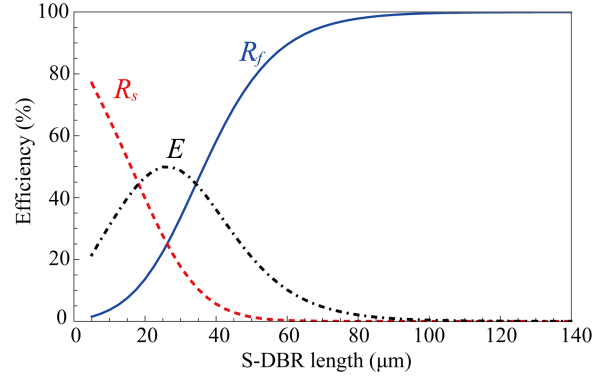

Fig. 3. Dependence of R_f, R_s, and E on S-DBR length.

normal DBR and the S-DBR, respectively. Here r_a and t_a are reflection and transmission coefficients on the assumption that no coupling occurs by the gratings, respectively. Then, $\kappa_{ga}, \kappa_{gs}, \alpha, E_{\nu a}^0, E_{\nu s}^0, \Delta$, and τ are coupling coefficients for couplings from the guided wave to the air- and substrate-radiation waves, the radiation decay factor of the FGC, normalized electric fields of the air- and substrate-radiation modes, a phase mismatch factor in z-direction between incident and radiation waves and photon lifetime in the waveguide resonator.

Equation (6) includes only radiation waves, whereas (7) includes multilayer reflection r_a as well. In the case of the designed F-CRIGF, $\kappa_{gs} = 0$ and $t_a = 0$ because of substrate reflection of 100% efficiency. Therefore, only terms of multilayer reflection and air radiation remain. The first and second terms of (8) show contributions from the radiation from the FGC and the leakage through both the DBRs, respectively. The specular reflectance R_s vanishes by substituting $\omega = \omega_{rc}$ and (8) into (7) when $R_{DBR} = R_{S-DBR} = 1$. Only R_f remains at λ_{rc} resultantly. When R_{DBR} and $R_{S-DBR} < 1$, the incident power is divided into a focusing reflection, a specular reflection, and the guided-wave leakage from the waveguide resonator. An extraction through the S-DBR is a portion of the guided-wave leakage. The extraction ratio E is given by

$$E = \{1 - (R_f + R_s)\} \times \frac{T_{S-DBR}}{T_{DBR} + T_{S-DBR}}, \qquad (10)$$

$$T_{DBR} = 1 - R_{DBR}, \qquad (11)$$

$$T_{S-DBR} = 1 - R_{S-DBR}, \qquad (12)$$

where T_{DBR} and T_{S-DBR} are transmittances of the normal DBR and S-DBR, respectively. The first and the second factors are the total leakage power and distribution ratio of the powers transmitted through the S-DBR. Fig. 3 shows the calculated dependences of R_f, R_s, and E on S-DBR length. The values of r_a, t_a, κ_{ga}, κ_{gs}, $E_{\nu a}^0$, $E_{\nu s}^0$ and Δ slightly vary in the FGC aperture due to incidence angle variation in a precise sense. In the calculation, we approximated these values as the ones for vertical incidence for simplicity. Longer S-DBR gives higher Q-factor of the ECDL but lower extraction efficiency. In other words, there is an optimal S-DBR length for the maximum efficiency of the guided-mode launching ECDL.
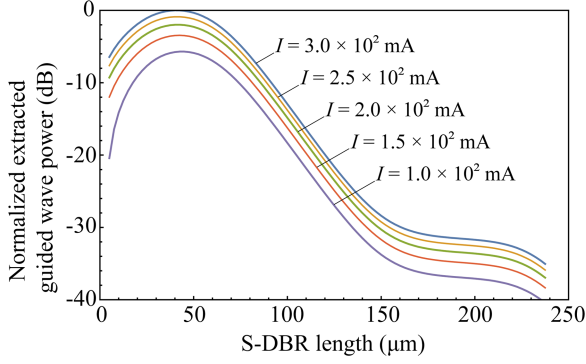
Fig. 4. Dependence of P_{ex} on S-DBR length.

Fig. 5. A SEM image of fabricated grating patterns.

Transmission power P_t from a typical Fabry-Perot laser through a front mirror is written by

$$P_t = \hbar\omega \frac{\tau_{ph} N_g c(1/L_a)\ln(1/R_1 R_2)}{1 + \sqrt{R_1/R_2}(1-R_1)/(1-R_2)} \frac{w_a L_a(J - J_{th})}{2q},$$

(13)

$$J_{th} = \frac{d_a q}{\tau_s}\left(D_0 + \frac{1}{\Gamma A_g N_g c \tau_{ph}}\right),$$

(14)

$$\frac{1}{\tau_{ph}} = N_g c\left\{\gamma_{int} + \left(\frac{1}{2L_a}\right)\ln\left(\frac{1}{R_1 R_2}\right)\right\},$$

(15)

where $\hbar, q, w_a, d_a, L_a, \Gamma, N_g, D_0, A_g, \tau_s, \tau_{ph}, \gamma_{int}, J, J_{th}, R_1$, and R_2 are the reduced Planck constant, the elementary charge, the width, thickness, and length of the active region, the confinement factor of the guided mode in the active region, a group refractive index of the guided mode, a transparency carrier density, a differential gain, a relaxation time of a spontaneous emission, a photon lifetime in the ECDL, an internal loss of the laser cavity, an injection current density, a threshold injection current density, and reflectances of front and back mirrors, respectively. The second and third factors of (13) are external differential quantum efficiency and the number of injection carrier, respectively. The threshold current density J_{th} is given by (14) showing that round-trip gain needs to beat round-trip cavity loss. The photon lifetime τ_{ph} is related with the internal and reflection losses as shown (15). We use the F-CRIGF as a front mirror, then $R_1 = R_f$. The incident power P_{in} to the F-CRIGF and the extracted power P_{ex} to the waveguide are given by

$$P_{in} = \frac{P_t}{1 - R_f},$$

(16)

$$P_{ex} = E P_{in},$$

(17)

We calculated dependence of P_{ex} on S-DBR length. We consider an SOA with R_2 of 0.9, w_a of 4 μm, d_a of 1.0 μm, L_a of 1000 μm, Γ of 0.035, N_g of 3.2, D_0 of 0.9×10^{18} cm^{-3}, A_g of 1.5×10^{-16} cm^2, τ_s of 3.5 ns, and γ_{int} of 0 mm^{-1}. Fig. 4 shows the calculated P_{ex} for several injection currents I, which is given by $J \times w_a L_a$. The S-DBR length for the maximum P_{ex} was about 50 μm in this case. On the other hand, longer S-DBR gives higher R_f and lower threshold injection current.
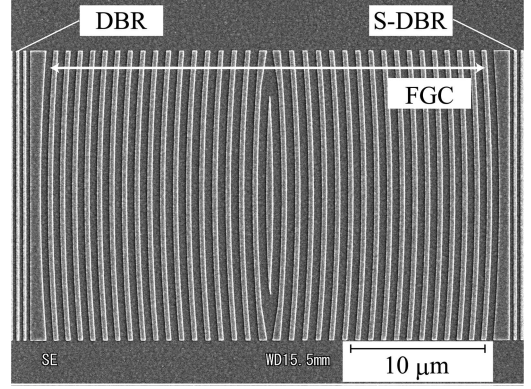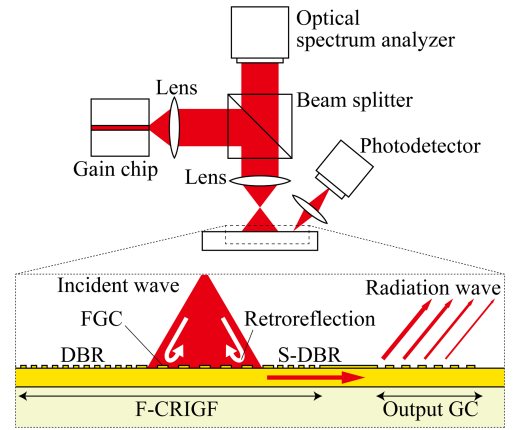

Fig. 6. Experimental setup to measure laser oscillation spectrum and the extracted power of the guided wave.

IV. FABRICATION AND EXPERIMENTAL RESULTS

A. Fabrication

The multilayer structure for the bottom mirror, waveguide, and gratings were deposited by radical assisted sputtering by Shincron Co., Ltd. The grating relief structure was formed by electron-beam (EB) direct writing lithography. The waveguide channel was obtained by remaining grating teeth. In other words, grating grooves and outside the channel were etched out. Fig. 5 shows a scanning electron microscope (SEM) image of grating patterns of the fabricated F-CRIGF.

B. Experimental Setup

A gain chip (SAF-1126-55-90-HTS, Thorlabs) was combined with the fabricated F-CRIGFs to construct ECDLs. We measured laser oscillation spectra and the extracted powers of the guided wave simultaneously. A schematic diagram of the experimental setup is shown in Fig. 6. An output GC was integrated next to the S-DBR for measuring P_{ex}. We inserted relay lenses and a beam splitter in order to measure lasing spectra by an optical spectrum analyzer. The emitted wave from the SOA was collimated, deflected by the beam splitter, and focused on the focal point of the F-CRIGF. The reflected wave returned to the SOA. Alignment tolerance is determined by the emission diameter of
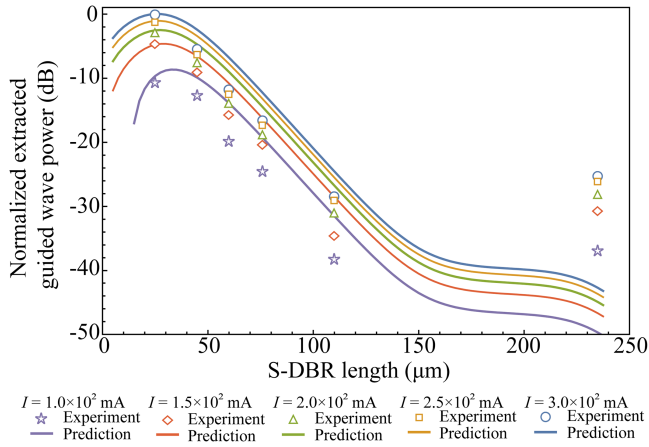
Fig. 7. Dependence of P_{ex} on S-DBR length with extra internal loss. The markers and lines show experimental and predicted values, respectively.

the SOA, typically a few micrometers. We should align the focal point of the F-CRIGF to the emission point. In the experiment, the F-CRIGF and the SOA were aligned actively for obtaining the highest laser power. Optical stages with micrometers were used, and the alignment accuracy was about 1 μm. Alignment error of 1 μm results in a mode-field matching ratio of -1 dB. Effect of this coupling loss is discussed below. The extracted guided wave from the F-CRIGF was out-coupled by the output GC, and was detected by a photodetector.

C. Experimental Results

Fig. 7 shows the measured dependences of P_{ex} on S-DBR length for several injection currents. The S-DBR length for the maximum extraction was shorter than the prediction shown in Fig. 4. This difference must be attributed to extra cavity loss caused by the insertion of optical components between the SOA and the F-CRIGF. The insertion loss should be counted in γ_{int} and can be written as

$$\gamma_{int} = \frac{1}{L_a} \ln \frac{1}{T_{lens}^2 \times R_{BS} \times \eta_c}, \qquad (18)$$

where T_{lens} is transmittance of the lenses, R_{BS} is reflectance of the beam splitter, and η_c is a mode-field matching ratio between emitted and returned waves at the end of the SOA. The estimated value of T_{lens}, R_{BS}, and η_c were 0.75, 0.90, and 0.8, respectively. The value of η_c was calculated on the assumption that the optical axis shift between the emitted wave and returned wave is 1 μm. We calculated the dependence of P_{ex} on S-DBR length with the γ_{int}. The calculated dependences are shown in Fig. 8 by lines and show good agreement with the experimental results. It is found that the fabricated F-CRIGF with S-DBR length of 25 μm gives the maximum extraction power.

Fig. 8 shows relationship between the measured laser power and the injection current for the F-CRIGF with the S-DBR length of 25 μm. The laser power was linearly increased from the threshold current of 50 mA. Fig. 9 shows the measured laser oscillation spectra. The peak wavelength did not shift and stayed at 1553 nm even when injection current increased. On the other hand, the oscillation bandwidth broadened. This broadening
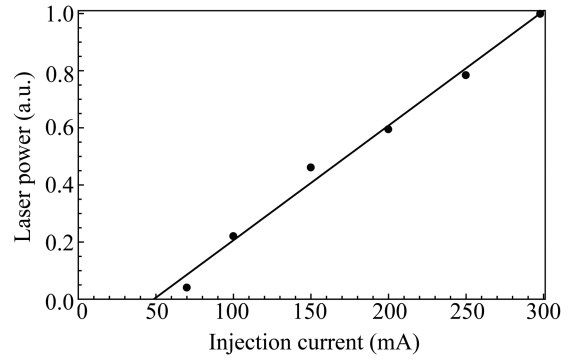

Fig. 8. Relationship between the measured laser power and the injection current.
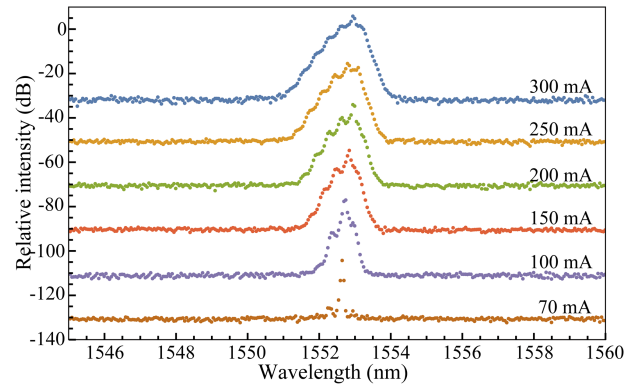

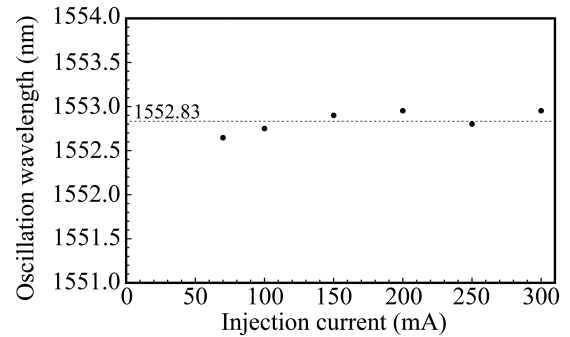Fig. 9. Laser oscillation spectra under different injection currents.

Fig. 10. Dependence of the peak wavelength on injection current. The line shows average wavelength.

means increase of longitudinal modes in oscillation. We cannot distinguish each longitudinal mode because the cavity length was extremely long. We can also see some small spikes corresponding to the longitudinal modes of a cavity length of 1 mm constructed by facets of the SOA. Fig. 10 shows the measured dependence of the peak wavelength on the injection current. The average wavelength was 1552.83 nm, and the fluctuation from the average was within 0.18 nm. It indicates that the F-CRIGF works well as a wavelength-stabilizing external laser mirror. Slight shifts of the oscillation wavelength from the designed λ_{rc} of 1550 nm can be attributed to the fabrication errors on the layer thickness and the grating fill factor.

V. Conclusion

We proposed an F-CRIGF serving as a wavelength-stabilizing laser mirror as well as a waveguide input coupler. We designed and fabricated the F-CRIGFs of the resonance wavelength of 1550 nm with several S-DBR lengths. We constructed ECDLs using the F-CRIGFs, and measured oscillation wavelengths and extracted guided wave powers. The dependences of the extracted powers on S-DBR length showed good agreement with the theoretically calculated results. The S-DBR length for the maximum extraction was shown to be 25 μm. We confirmed simultaneous wavelength stabilized lasing and input coupling even though some extra optical components were inserted in the laser cavity for experimental characterization.

Acknowledgment

References

[1] L. Mashev and E. Popov, "Zero order anomaly of dielectric coated gratings," *Opt. Commun.*, vol. 55, no. 6, pp. 377–380, Oct. 1985.

[2] R. Magnusson and S. S. Wang, "New principle for optical filters," *Appl. Phys. Lett.*, vol. 61, no. 9, pp. 1022–1024, Jun. 1992.

[3] S. S. Wang and R. Magnusson, "Theory and applications of guided-mode resonance filters," *Appl. Opt.*, vol. 32, no. 14, pp. 2606–2613, May 1993.

[4] S. M. Norton, T. Erdogan, and G. M. Morris, "Coupled-mode theory of resonant-grating filters," *J. Opt. Soc. Amer. A*, vol. 14, no. 3, pp. 629–639, Mar. 1997.

[5] D. Rosenblatt, A. Sharon, and A. A. Friesem, "Resonant grating waveguide structures," *IEEE J. Quantum Electron.*, vol. 33, no. 11, pp. 2038–2059, Nov. 1997.

[6] Z. S. Liu, S. Tibuleac, D. Shin, P. P. Young, and R. Magnusson, "High-efficiency guided-mode resonance filter," *Opt. Lett.*, vol. 23, no. 19, pp. 1556–1558, Oct. 1998.

[7] Z. Hegedus and R. Netterfield, "Low sideband guided-mode resonant filter," *Appl. Opt.*, vol. 39, no. 10, pp. 1469–1473, Apr. 2000.

[8] S. Block, E. Gamet, and F. Pigeon, "Semiconductor laser with external resonant grating mirror," *IEEE J. Quantum Electron.*, vol. 41, no. 8, pp. 1049–1053, Aug. 2005.

[9] R. A. Sims et al., "Spectral narrowing and stabilization of thulium fiber lasers using guided-mode resonance filters," *Opt. Lett.*, vol. 36, no. 5, pp. 737–739, Mar. 2011.

[10] A. A. Mehta, R. C. Rumpf, Z. A. Roth, and E. G. Johnson, "Guided mode resonance filter as a spectrally selective feedback element in a double-cladding optical fiber laser," *IEEE Photon. Technol. Lett.*, vol. 19, no. 24, pp. 2030–2032, Dec. 2007.

[11] Y. Li et al., "Guided-mode resonance filters for wavelength selection in mid-infrared fiber lasers," *IEEE Photon. Technol. Lett.*, vol. 24, no. 24, pp. 2300–2302, Dec. 2012.

[12] Y. Zhou, M. Moewe, J. Kern, M. C. Y. Huang, and C. J. Chang-Hasnain, "Surface-normal emission of a high-Q resonator using a subwavelength high-contrast grating," *Opt. Exp.*, vol. 16, no. 22, pp. 17282–17287, Oct. 2008.

[13] C. J. Chang-Hasnain, Y. Zhou, M. C. Y. Huang, and C. Chase, "High-contrast grating VCSELs," *IEEE J. Sel. Top. Quantum Electron.*, vol. 15, no. 3 pp. 869–878, May/Jun. 2009.

[14] I. Avrutsky and R. Rabady, "Waveguide grating mirror for large-area semiconductor lasers," *Opt. Lett.*, vol. 26, no. 13, pp. 989–991, Jul. 2001.

[15] S. Song, F. Sun, Q. Chen, and Y. Zhang, "Narrow-linewidth and high-transmission terahertz bandpass filtering by metallic gratings," *IEEE Trans. Terahertz Sci. Technol.*, vol. 5, no. 1, pp. 131–136, Jan. 2015.

[16] A. Ferraro, A. A. Tanga, D. C. Zografopoulos, G. C. Messina, M. Ortolani, and R. Beccherelli, "Guided mode resonance flat-top bandpass filter for terahertz telecom applications," *Opt. Lett.*, vol. 44, no. 17, pp. 4239–4242, Sep. 2019.

[17] C. Wang and S. D. Lin, "Resonant cavity-enhanced quantum-dot infrared photodetectors with guided-mode resonance reflector," in *Proc. IEEE Conf. Lasers Electro-Opt. Pacific Rim*, 2013, pp. 1–2.

[18] M. Huang, Y. Zhou, and C. J. Chang-Hasnain, "A surface-emitting laser incorporating a high-index-contrast subwavelength grating," *Nature Photon.*, vol. 1, pp. 119–122, Feb. 2007.

[19] Y. Kanamori, M. Shimono, and K. Hane, "Fabrication of transmission color filters using silicon subwavelength gratings on quartz substrates," *IEEE Photon. Technol. Lett.*, vol. 18, no. 20, pp. 2126–2128, Oct. 2006.

[20] Y.-T. Yoon, H.-S. Lee, S.-S. Lee, S. H. Kim, J.-D. Park, and K.-D. Lee, "Color filter incorporating a subwavelength patterned grating in poly silicon," *Opt. Exp.*, vol. 16, no. 4, pp. 2374–2380, Feb. 2008.

[21] Y.-T. Yoon, C.-H. Park, and S.-S. Lee, "Highly efficient color filter incorporating a thin metal–dielectric resonant structure," *Appl. Phys. Exp.*, vol. 5, no. 2, Feb. 2012, Art. no. 022501.

[22] E.-H. Cho et al., "Two-dimensional photonic crystal color filter development," *Opt. Exp.*, vol. 17, no. 10, pp. 8621–8629, May 2009.

[23] H. Lochbihler, "Colored images generated by metallic sub-wavelength gratings," *Opt. Exp.*, vol. 17, no. 14, pp. 12189–12196, Jul. 2009.

[24] M. Grande et al., "Graphene-based absorber exploiting guided mode resonances in one-dimensional gratings," *Opt. Exp.*, vol. 22, no. 25, pp. 31511–31519, Dec. 2014.

[25] H. L. Chen et al., "A 19.9%-efficient ultrathin solar cell based on a 205-nm-thick GaAs absorber and a silver nanostructured back mirror," *Nature Energy*, vol. 4, pp. 761–767, Aug. 2019.

[26] B. Cunningham, P. Li, B. Lin, and J. Pepper, "Colorimetric resonant reflection as a direct biochemical assay technique," in *Proc. IEEE Int. Conf. 15th IEEE Int. Conf. Micro Electro Mech. Syst.*, 2002, pp. 64–68.

[27] M. El Beheiry, V. Liu, S. Fan, and O. Levi, "Sensitivity enhancement in photonic crystal slab biosensors," *Opt. Exp.*, vol. 18, no. 22, pp. 22702–22714, Oct. 2010.

[28] K. J. Lee et al., "Silicon-layer guided-mode resonance polarizer with 40-nm bandwidth," *IEEE Photon. Technol. Lett.*, vol. 20, no. 22, pp. 1857–1859, Nov. 2008.

[29] M. Mutlu, A. E. Akosman, and E. Ozbay, "Broadband circular polarizer based on high-contrast gratings," *Opt. Lett.*, vol. 37, no. 11, pp. 2094–2096, Jun. 2012.

[30] G. Biener, A. Niv, V. Kleiner, and E. Hasman, "Computer-generated infrared depolarizer using space-variant subwavelength dielectric gratings," *Opt. Lett.*, vol. 28, no. 16, pp. 1400–1402, Aug. 2003.

[31] I. Vartiainen, J. Tervo, and M. Kuittinen, "Depolarization of quasi-monochromatic light by thin resonant gratings," *Opt. Lett.*, vol. 34, no. 11, pp. 1648–1650, Jun. 2009.

[32] S. Ura, J. Inoue, K. Kintaka, and Y. Awatsuji, "Proposal of small-aperture guided-mode resonance filter," in *Proc. 13th Int. Conf. Transparent Opt. Netw.*, 2011, pp. 1–4.

[33] K. Kintaka, T. Majima, J. Inoue, K. Hatanaka, J. Nishii, and S. Ura, "Cavity-resonator-integrated guided-mode resonance filter for aperture miniaturization," *Opt. Exp.*, vol. 20, no. 2, pp. 1444–1449, Jan. 2012.

[34] J. Inoue et al., "Aperture miniaturization of guided-mode resonance filter by cavity resonator integration," *Appl. Phys. Exp.*, vol. 5, no. 2, Jan. 2012, Art. no. 022201.

[35] A. Tsuji, J. Inoue, K. Nishio, S. Ura, and K. Kintaka, "Integrated optic device for narrow-band reflection and guided-wave launching," in *Proc. IEEE CPMT Symp. Jpn.*, 2016, pp. 177–180.

[36] J. Inoue, A. Tsuji, K. Kintaka, K. Nishio, and S. Ura, "Wavelength division multiplexer based on cavity-resonator-integrated guided-mode resonance filters for a compact multi-wavelength light source," *Opt. Exp.*, vol. 26, no. 3, pp. 2212–2219, Feb. 2018.

[37] J. Inoue, T. Kusuura, R. Ueda, K. Kintaka, and S. Ura, "Narrowband focusing retroreflector with a thin-film structure," *Appl. Phys. Exp.*, vol. 14, no. 8, Jul. 2021, Art. no. 082003.

[38] R. Ueda et al., "Laser-wavelength stabilization by a focusing cavity-resonator-integrated guided-mode resonance filter," in *Proc. IEEE 26th Microoptics Conf.*, 2021, pp. 1–2.

[39] A. Katzir, A. C. Livanos, and A. Yariv, "Chirped grating demultiplexers in dielectric waveguides," *Appl. Phys. Lett.*, vol. 30, no. 10, pp. 519–521, Aug. 1977.

[40] D. Heitmann and R. V. Pole, "Two dimensional focusing holographic grating coupler," *Appl. Phys. Lett.*, vol. 37, no. 7, pp. 585–587, Jul. 1980.

[41] J. Inoue, T. Kusuura, K. Akamatsu, and S. Ura, "Design of a narrowband retroreflector based on guided-mode resonance," *J. Opt. Soc. Amer. B*, vol. 37, no. 4, pp. 579–583, Apr. 2020.